

Kinetics of Light-Responsive CNT / PNIPAM Hydrogel Microactuators

Aoife Gregg, Michael De Volder, and Jeremy J. Baumberg*

Light-responsive microactuators composed of vertically aligned carbon nanotube (CNT) forests mixed with poly(N-isopropylacrylamide) (PNIPAM) hydrogel composites are studied. The benefit of this composite is that CNTs act as a black absorber to efficiently capture radiative heating and trigger PNIPAM contraction. In addition, CNT forests can be patterned accurately using lithography to span structures ranging from a few micrometers to several millimeters in size, and these CNT-PNIPAM composites can achieve response times as fast as 15 ms. The kinetics of these microactuators are investigated through detailed analysis of high-speed videos. These are compared to a theoretical model for the deswelling dynamics, which combines thermal convection and polymer diffusion, and shows that polymer diffusion is the rate-limiting factor in this system. Applications of such CNT/hydrogel actuators as microswimmers are discussed, with light-actuating micro-jellyfish designs exemplified, and >1500 cycles demonstrated.

lengthscales (micro- to millimeters) while the anisotropic properties arising from the alignment of CNTs allow for redirecting the isotropic expansion of PNIPAM into an anisotropic reconfiguration. Here, the kinetics of contraction (“deswelling”) in these composite microactuators are investigated in order to understand the physical behaviors of this system, and to predict how actuation speeds can be programmed.

The active material of these actuators is PNIPAM, a temperature-responsive polymer, which can be crosslinked into a hydrogel with a reversible size change of more than 50%.^[2] PNIPAM is a lower critical solution temperature (LCST) polymer with a critical temperature (T_c) of ≈ 32 °C, above which it is no longer hydrophilic and so preferentially interacts with other PNIPAM strands, expelling water and

1. Introduction

Carbon nanotubes (CNTs) and PNIPAM hydrogel have previously been combined to make a microactuator system that is responsive to light and can demonstrate a wide range of programmable shape deformations. In particular, vertically aligned CNTs forests are known to have an emissivity close to 1 across a wide range of wavelengths, making it an ideal material for heating by radiation and triggering a volume change of PNIPAM hydrogels (see below).^[1] In addition, CNT forests can be patterned by lithography to create structures with shapes spanning wide

contracting. When its temperature is lowered back below T_c , it absorbs water and reswells to its original size.^[3,4] However, PNIPAM is typically limited by its slow response time, its responsiveness only to heat, and the challenge of transforming its isotropic (de)swelling into useful deformations.^[5,6] Similar problems are faced with other hydrogels, and the typical approach to addressing these challenges is to combine them with an additional material.^[7]

Carbon nanotubes (CNTs) are well known for their remarkable strength, with Young’s modulus of up to 1 TPa and an inherent tensile strength of over 100 GPa.^[8–10] They are highly durable and resistant to fatigue over millions of strain cycles.^[11,12] Vertically aligned forests of CNTs (VACNTs) can be grown by chemical vapor deposition, and these forests can be produced in predefined patterns by depositing the growth catalyst in any desired pattern using lithography.^[13] While CNTs add many useful properties, such as higher electrical and thermal conductivity and improved mechanical strength, two key features added by CNTs here are their optical absorptivity and anisotropic mechanical properties. VACNTs act as black bodies, absorbing up to 99% of light over a wide wavelength range from UV to far IR.^[14,15] This means that the CNTs in the composite hydrogel absorb light and locally convert it to heat, which is transferred to the surrounding PNIPAM. With sufficient irradiation power, PNIPAM is heated above T_c and contracts. Combining CNTs with PNIPAM enables a light-triggered response, opening up the use of microactuators to more applications, since bulk heating of the microactuator environment to drive actuation is often not feasible. The use of light as a stimulus also speeds up response times, as the

A. Gregg, J. J. Baumberg
Cavendish Laboratory
Department of Physics
University of Cambridge
J.J. Thomson Avenue, Cambridge CB3 0HE, UK
E-mail: jjb12@cam.ac.uk

A. Gregg, M. De Volder
Institute for Manufacturing
Department of Engineering
University of Cambridge
17 Charles Babbage Road, Cambridge CB3 0FS, UK

 The ORCID identification number(s) for the author(s) of this article can be found under <https://doi.org/10.1002/smll.202305034>

© 2023 The Authors. Small published by Wiley-VCH GmbH. This is an open access article under the terms of the Creative Commons Attribution License, which permits use, distribution and reproduction in any medium, provided the original work is properly cited.

DOI: 10.1002/smll.202305034

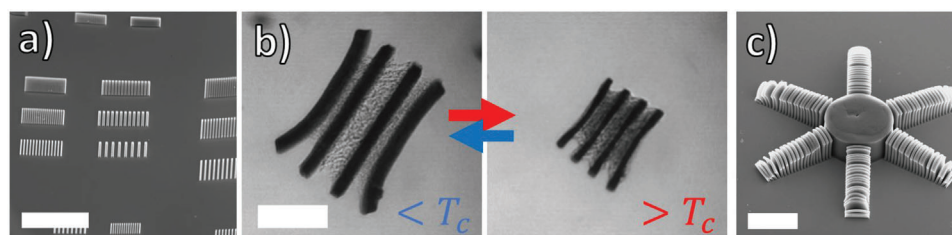


Figure 1. a) Scanning electron microscopy image of VACNT structures, shaped into arrays of walls. b) Optical microscopy images showing the reversible contraction of CNT/PNIPAM hydrogel actuators. Black regions are CNT/PNIPAM hydrogel composite, and translucent regions between the walls are bulk PNIPAM hydrogel. c) Scanning electron micrograph of VACNT forests patterned into jellyfish design. Scale bars are 500 μm , 150 μm , and 250 μm respectively.

actuator itself is selectively heated rather than heating the entire environment. This also reduces the energy requirements of the actuator system. Since the anisotropic mechanical properties of CNTs are maintained in the CNT/PNIPAM hydrogel composites, anisotropic shape changes can be achieved during actuation. The use of CNT skeletons allows for molding the hydrogel into desired shapes, making it straightforward to achieve complex designs with size ranges over 3 orders of magnitude, from 10 μm to >1 cm.^[1] This ability to construct microscale actuators also allows for a faster response, because actuation timescales shorten with the reduced distance over which water being expelled/absorbed must be transported.

Here, the kinetics of the CNT/PNIPAM hydrogel actuator contraction is investigated by analyzing the actuator size over time when optically heated. The speed of actuation is found to be limited by phase separation within the hydrogel, rather than heat transfer through the CNTs. Many models for the kinetics of PNIPAM deswelling have been described^[2,16–21]; here, these existing strategies are applied to this novel CNT/PNIPAM hydrogel composite system. While previous studies have established the mechanics of photoresponsive actuators in general,^[22,23] the structuring of the vertically aligned CNTs introduces new complexity into the composite material. We show how simple models are unable to account for the observations, and show that the crucial aspect to include (in the simplest way) is the polymer diffusion. The resulting model is used to suggest approaches for increasing actuation speeds, including higher laser powers for actuation, decreasing actuator size, and reducing phase separation. Potential applications for CNT/PNIPAM hydrogel microactuators are discussed, including a demonstration of excellent cyclability (>1500 cycles) and jellyfish-like actuation.

2. Results and Discussion

2.1. Experimental Data

CNT/PNIPAM hydrogel microactuators are composed of arrays of VACNT forests shaped into walls (Figure 1a). In these structures, PNIPAM hydrogel is present both within the VACNT forests (forming a CNT/hydrogel composite region) and between the walls (forming a bulk hydrogel region) (Figure 1b).^[1] The structure is actuated here by illuminating with a 532 nm laser over a range of powers (40–200 mW, resulting in irradiance 10–55 W cm^{-2}) so that the CNTs absorb light and heat the structure above T_c (Figure 1b). High speed videos (250 fps) of the actu-

ator contraction are recorded using a fast camera (Photron FAST-CAM Mini UX100) attached to a microscope (see Methods), and analyzed frame-by-frame to extract the area of each actuator over time while undergoing laser heating. As seen below, the dynamics do not simply follow an exponential decay, hence the various processes need to be considered.

2.2. Diffusion Model

We first discuss how such composite hydrogels would be expected to expand and contract, to identify the key parameters in their dynamic response. The kinetics of swelling and deswelling of hydrogels was discussed by Tanaka et al,^[24–27] in which the expected radius of a spherical hydrogel over time, $a(t)$, was derived. In brief, the displacement vector $\mathbf{u}(\mathbf{r}, t)$ of a given point within the polymer network from its equilibrium position is bounded by $\mathbf{u}(\mathbf{r} = 0, t \rightarrow \infty) = 0$, and given by

$$f \frac{\partial \mathbf{u}}{\partial t} = \nabla \cdot \bar{\sigma} \quad (1)$$

where $\bar{\sigma}$ is the stress tensor and f is the coefficient of friction between the polymer network and the solvent. The left-hand side of Equation (1) is the force on the hydrogel due to friction and the right-hand side is the net force from the hydrogel internal stresses. Taking the strain tensor $u_{ik} = \frac{1}{2} \left(\frac{\partial u_k}{\partial x_i} + \frac{\partial u_i}{\partial x_k} \right)$, $\bar{\sigma}$ can be related to \mathbf{u} by

$$\sigma_{ik} = K \nabla \cdot \mathbf{u} \delta_{ik} + 2 \mu \left(u_{ik} - \frac{1}{3} \nabla \cdot \mathbf{u} \delta_{ik} \right) \quad (2)$$

where K is the bulk modulus, μ is the shear modulus. The first term describes the stress resulting from volume changes and the second describes the stress resulting from shear deformations. Assuming a spherical gel, so $\mathbf{u}(\mathbf{r}, t) = u(r, t)(\mathbf{r}/r)$, Equation (1) becomes

$$\frac{\partial u}{\partial t} = D \frac{\partial}{\partial r} \left(\frac{1}{r^2} \left[\frac{\partial}{\partial r} (r^2 u) \right] \right) \quad (3)$$

where D is the collective diffusion coefficient of the polymer network, in an ideal case given by the Tanaka-Fillmore equation^[25]:

$$D = \frac{1}{f} (K + 4\mu/3) \quad (4)$$

Using initial condition $u(r, 0) = \Delta a_0(r/a)$, where $\Delta a_0 = a - a_i$, with final radius a , initial radius a_i , boundary condition $\sigma_{\perp} = 0$ normal to the gel surface, and $\mu \ll K$, Equation (3) can be solved as a Fourier series,^[25]

$$a(t) = a - \Delta a_0 \sum_{n=1}^{\infty} \frac{6}{\pi^2 n^2} \exp\left(\frac{-n^2 t}{\tau}\right) \quad (5)$$

where τ is the characteristic response time, given by

$$\tau = a^2 / D \quad (6)$$

It is notable that D is dependent on temperature in a wide range of ways, as each of K , μ , and f change with both temperature and the internal structure of the hydrogel. Developing an understanding of this dependence is a key point of discussion in this work.

2.3. Hybrid Kinetic Model

In order to investigate the coupling of heat transfer and diffusion, a simple physical model for the actuator is used to predict the deswelling dynamics. Initially, the model assumes diffusion is fast enough to not influence with heat transfer limiting the response (which is subsequently shown to be incorrect below). In this case, the actuator size $a(T)$ is determined by the product of the initial actuator size and the expected swelling ratio for the PNIPAM hydrogel at each temperature (Figure S1, Supporting Information). The deswelling dynamics are then set by the temperature of the actuator over time as it is heated by the laser. This combines optical heating (assuming the actuator fully absorbs all incident laser flux) and heat loss predominantly due to convection, giving for linear size $a(T)$,

$$C_V V(a) \frac{dT}{dt} = P A_{\text{CNT}}(a) - H_c A_s(a) (T - T_e) \quad (7)$$

where P is the irradiance from laser heating (in $\text{J s}^{-1} \text{m}^{-2}$), A_{CNT} is the actuator area facing the laser, which contains CNTs while A_s is the total actuator surface area, H_c is the convective heat transfer coefficient, $T - T_e$ is the temperature difference between the actuator and its environment (assumed to be 21°C throughout), V is the actuator volume, and C_V is the volumetric heat capacity of the actuator (in $\text{J K}^{-1} \text{m}^{-3}$), taken to be the heat capacity of water. It is assumed that the temperature is constant throughout the actuator.

Since A and V vary with time and temperature, analytic solutions of Equation (7) are not available. Instead for simulations, the temperature calculated at each successive time step using a first-order forward Euler method, is

$$T_{n+1} = T_n + \left[\frac{P A_{\text{CNT}}(a_n) - H_c A_s(a_n) (T_n - T_e)}{V(a_n) C_V} \right] \quad (8)$$

Approximating a cuboid actuator for A_{CNT} , A_s and V , we adjust V , H_c to best fit all the experiments, since the fill factor of PNIPAM within the CNT skeleton is hard to measure. The dimensions of the $70 \mu\text{m}$ high actuator are shown in Figure 1b. The

height of the actuator remains constant over time as the aligned CNTs prevent vertical deformation.^[1] The convection coefficient H_c is varied between $50\text{--}3000 \text{ W m}^{-2} \text{ s}^{-1}$, typical for objects in water. This heat-transfer-only model is used fit to the experimental data using differential evolution methods (*scipy optimize* package), a global minimization that finds the best fixed parameters for the whole dataset. We note that the fitting parameters here effectively act together as one combined scaling factor, so individual values are not independently reliable.

The optical heating rate reduces over time as the actuator shrinks (intersecting less laser light, included in the model by the change in A_{CNT}), while convective heat loss increases over time as the temperature difference between the actuator and the environment increases. The stable equilibrium temperature thus varies with laser power.

We thus now compare the model with experiments on a microactuator (Figure 1b) illuminated at different powers, giving characteristic dynamical evolution (Figure 2, dashed). When the temperature dynamics are combined with the temperature-dependent swelling ratio of PNIPAM from literature, the best-fit deswelling curves reproduce many features of the experimental data, but overall do not match sufficiently (Figure 2a). Initial decay times agree well, but then overestimate the speed at which the fully-contracted volume is reached, particularly at lower laser powers. This suggests that a heat transfer-only model does not adequately describe the contraction kinetics of CNT/PNIPAM hydrogel actuators.

To improve this analysis of deswelling, polymer diffusion effects are added to the model. These are taken into account using the Tanaka model discussed above, although equations (5,6) are formulated for a constant temperature. We thus use the equilibrium ($t \gg \tau$) actuator size $a_{\infty}(T)$ at the current temperature T , extracted from the swelling ratio of PNIPAM with temperature (Figure S1, Supporting Information). Updating the actuator size at each time step uses the current temperature from equation (8). Approximating a cuboid actuator for A_{CNT} , A_s and V , we obtain

$$a_{n+1} = a_{\infty}(T_n) + [a_n - a_{\infty}(T_n)] \sum_{n=1}^{\infty} \frac{6}{\pi^2 n^2} \exp\left\{\frac{-n^2 dt}{\tau(a_n)}\right\} \quad (9)$$

where the characteristic response time $\tau = a_n^2 / D(a)$ sensitively affects the actuator behavior via the choice of diffusion parameter $D(a)$. Now that the diffusion time is taken into account, the actuator size is dependent on both temperature and time as $a(t, T)$. Simulations combining equations (8) and (9) thus describe both the dynamics of heating and the polymer diffusion, across the PNIPAM transition.

Initially assuming constant diffusion $D(a) = D_0$ slightly improves the model agreement, particularly at the transition between fast and slow deswelling regimes, but overall still does not fit (Figure 2b). Similar results are obtained for any model where diffusion increases with temperature, despite the intuition for decreasing the viscosity of water when heated (decreasing the friction f between the polymer and solvent) and increasing bulk modulus of PNIPAM across T_c .^[28,29]

In contrast to these conventional approaches, diffusion in PNIPAM hydrogels has been shown to slow during deswelling as a result of internal phase separation between swollen gel

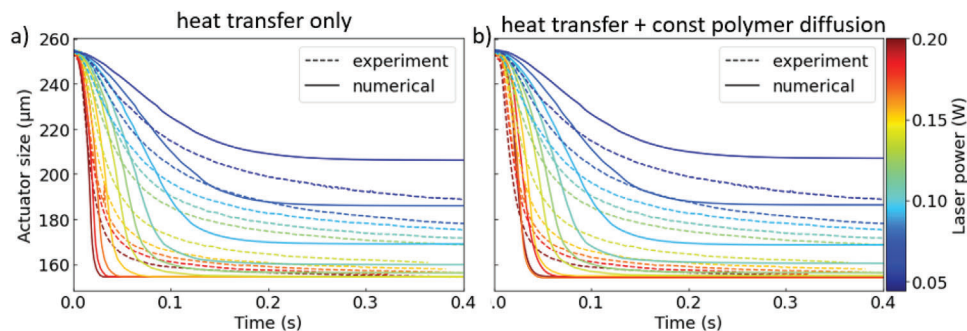


Figure 2. Deswelling of a CNT/hydrogel microactuator over time for laser powers from 45–200 mW, comparing experimental (dashed lines) results with a) kinetic model based solely on heat transfer (solid lines), or b) heat transfer and a constant polymer network diffusion (solid lines).

regions, collapsed gel regions, and solvent.^[16,30,31] Phase separation within the hydrogel is visible as an increase in opacity, visible in the CNT/PNIPAM hydrogel microactuators below and above T_c (Figure 1b). This diffusion is thus nonlinear with gel volume, reducing D quickly at early stages of deswelling and reaches a constant small value at the final stages of deswelling. Taking a power law dependence of the form

$$D(a) \propto \left[\frac{V(a) - V_\infty}{V_\infty} \right]^\nu \quad (10)$$

where V_∞ is the final volume ($t \rightarrow \infty$), we find the best-fit diffusion model now accurately reproduces the experimental results (Figure 3a) giving a fitting exponent $\nu = 1.05 \pm 0.05$ (the uncertainty in ν is determined by the sensitivity of the fit quality to choice of ν , Figure S2, Supporting Information). This shows the significant influence of diffusion on the deswelling kinetics, as without it (blue line) a much faster dynamics is predicted. Similar dynamics are then retrieved for the temperature extracted from the model (Figure 3b), while the diffusion rate drops rapidly (Figure 3c) as soon as the temperature reaches T_c (after 40 ms).

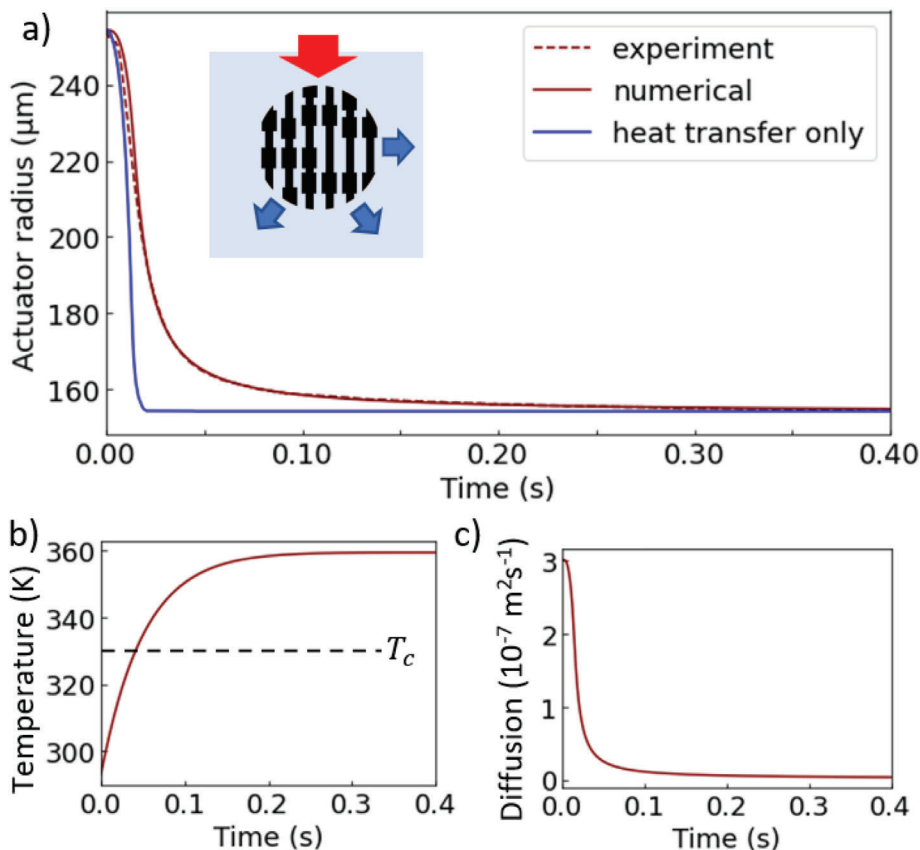


Figure 3. a) Deswelling of CNT/hydrogel microactuator vs time for 55 Wcm^{-2} laser power, compared to a kinetic model combining heat transfer with the diffusion of a polymer network in different phases (inset). The evolution of size of the actuator without diffusion terms is also shown (blue solid line). b) Temperature and c) polymer diffusion constant of actuator vs time, extracted from the model in (a).

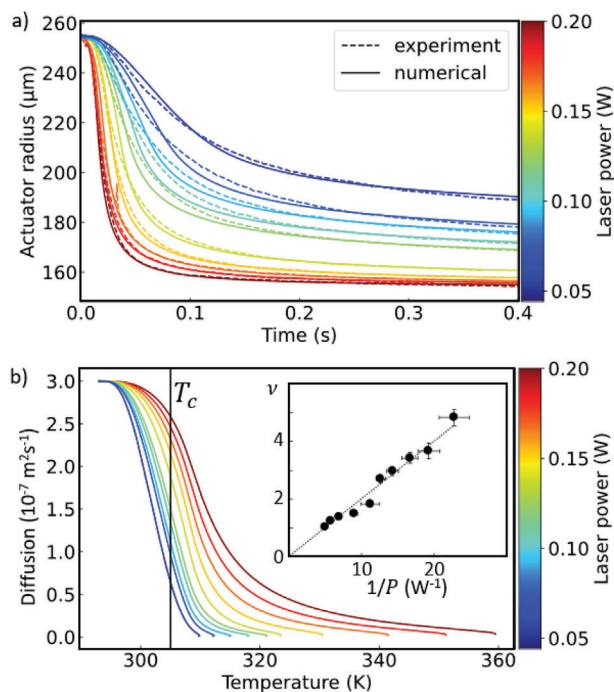


Figure 4. a) Deswelling of CNT/hydrogel microactuator vs time for laser powers from 45–200 mW, comparing experimental (dashed) with model kinetics (solid lines) combining heat transfer and polymer diffusion decreasing with actuator shrinkage. b) Extracted average diffusion rate of polymer network as temperature increases, for different laser powers, with T_c marked. Inset: Extracted nonlinear diffusion exponent ν vs inverse laser power.

Fitting this model to all laser powers generates reasonably matched deswelling curves (Figure 4). This can only be achieved by linearly decreasing ν from 4.8 to 1.0 as the laser power increases (Figure 4b inset). Since the heating rate and final temperature reached are both directly proportional to the laser power (Figure S3, Supporting Information), this ν dependence indicates that the influence of phase separation decreases with increasing heating rate. This suggests that increasing heating rate either reduces the density of phase-separated domains, produces more efficient fractal diffusion channels, or results in faster homogenization of separate phases (or some combination of all). It is likely that the assumption of constant temperature throughout the actuator could also fail at higher heating rates due to the time taken to transfer heat from the composite regions to the bulk regions, which may affect the validity of our model. Such heterogeneity could also affect phase separation, by allowing the cooler bulk PNIPAM regions to enhance phase separation by acting as channels for water transfer. We note that at lower laser powers (low heating rates) the fit quality reduces, likely because these approximations become less adequate, such as the swelling ratio calibration for PNIPAM hydrogels (Figure S1, Supporting Information), laser spot uniformity, dynamics of phase separation and homogenization, and differences between CNT/PNIPAM hydrogel composites and bulk PNIPAM hydrogels (Figure S4, Supporting Information).

The measurements shown here are repeated on a range of CNT/PNIPAM hydrogel composite actuator geometries, with dif-

ferent aspect ratios, CNT filling fractions, CNT heights, and PNIPAM cross-linking. In all cases, similar dynamics are found, with variations that are not yet fully systematic (Figure S5, Supporting Information). This likely reflects insufficient control over the PNIPAM morphology and cross-linking in CNT forests. Further work is thus of significant interest, since the geometry is fully scalable and can thus be optimized for high-speed actuation. So far, the fastest response times to deswell from 10% to 75% of its full contraction ≈ 15 ms.

Since this model well reproduces the experimental data, we now explore various strategies for reducing the contraction time of CNT/PNIPAM hydrogel microactuators. A faster response time is predicted by reducing the size of the actuator, by increasing the optical power used for optical heating, increasing the background temperature, or by eliminating the effect of phase separation (Figure 5). This suggests future work to improve microactuator response times should concentrate on decreasing actuator sizes to the minimum size possible for the selected application (Figure S6, Supporting Information, though this depends on the desired application) and strategies for reducing phase separation, such as increasing porosity to create more interconnected water transport pathways. A range of techniques could be used to increase porosity, including changing crosslinker concentrations and using RAFT polymerization.^[32–34] For machinery applications, the force stroke is most dependent on the initial response upon heating across the LCST, with the polymer diffusion then only roughly doubling the response time. Here, the response time t_r is defined to be the time elapsed between 10% and 75% of the full actuation, chosen to capture the dominant steep contraction stage rather than the slower starting and final stages of the contraction.

2.4. Demonstrations of CNT/Hydrogel Actuators

The CNT/PNIPAM microactuator system provides a set of features that are encouraging for a range of applications: the ability to fabricate complex shapes at small scales across a very flexible design space, high-density fabrication that scales by simultaneously manufacturing of 100–10 000 microactuators per chip (Figure S7, Supporting Information), and the ability to control actuation by either heat or light. Another key property, which is important for any application is the cyclability of the system.

As CNTs have been shown to have excellent fatigue resistance^[10] and CNT-PNIPAM hydrogels have previously been shown to maintain actuation over 1200 cycles,^[35] good cyclability is expected for these composite actuators. This was tested by repeatedly laser heating a microactuator and allowing it to cool, capturing an image of it at each step. The actuator areas extracted from these images show excellent consistency in both cold and hot states for 1650 cycles over 100 h (Figure 6) with no visible damage to the actuator (Figure S8, Supporting Information). The main reason for variations in area, particularly in early cycles, is instability in the position of the actuator within the frame as it rotates and moves slightly out of focus. However, this stabilizes within the first 100 cycles, while the presence of occasional outliers does not affect the overall trend. A linear fit of these results suggests a degradation of the actuation to 80% of its original magnitude after more than 8000 cycles.

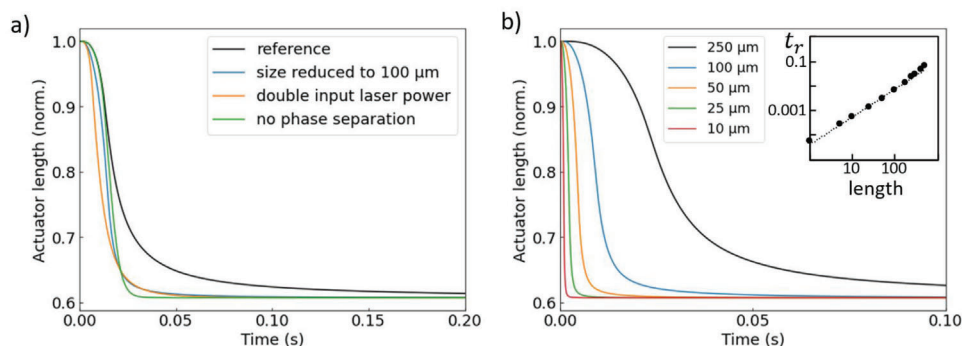


Figure 5. Predicted deswelling for modified CNT/PNIPAM hydrogel actuators. a) Effects of reducing initial actuator size, doubling the laser power, or turning off the effect of phase separation in the simulation. Reference curve at 55 W cm^{-2} laser power. b) Predictions for actuators of various starting sizes (assuming cube-shaped actuators). Inset: response times t_r from predicted deswelling curves (details in Figure S6, Supporting Information).

However, microactuators may survive much longer than this as the measurements here are sensitive to artifacts in imaging, actuator drift, and stability, rather than only revealing material degradation.

One potential application of CNT/PNIPAM hydrogel microactuators is as microswimmers: microscale structures, which can move autonomously in liquid. These have been extensively discussed for the past two decades,^[36] but their implementation has been difficult and limited. The struggle to create microswimmers originates in their low Reynolds number ($Re = \rho u L / \mu$) which is the ratio of inertial to viscous forces, for fluid density ρ , speed u , micro-swimmer size L , and dynamic viscosity μ . Fluid flow is turbulent at high Re and laminar at low Re . For typical microswimmers in water ($L = 100 \mu\text{m}$, $u = 100 \mu\text{m s}^{-1}$, $\rho = 1000 \text{ kg m}^{-3}$, $\mu = 0.001 \text{ N s m}^{-2}$), $Re \approx 0.01$ is in the laminar regime introducing the

‘scallop problem’. Famously described by Purcell in 1977,^[37] this identifies the challenge of swimming in low Re as the reversibility curse: when fluid flow is caused by the motion of a structure, reversing that motion causes exactly the opposite fluid flow. The only way to achieve translational swimming with a microswimmer is to create movements that are not time-symmetric,^[37,38] composed either of continuous ‘forward’ movement, or forward and reverse strokes tracing different paths.

PNIPAM is promising as an active material for microswimmers with different forward/reverse strokes as a result of its ability to operate out-of-equilibrium^[39] and the differing water transport in swelling and deswelling stages. The latter has been demonstrated via observation of phase separation upon deswelling, but not swelling.^[16] Observing CNT/PNIPAM hydrogel actuators shows they indeed travel a different path upon swelling and deswelling (Figure S9, Supporting Information), which suggests that they may be appropriate for the fabrication of microswimmers. Potential explanations for this asymmetry include this difference in phase separation and the difference in heat transfer mechanisms between the swelling and deswelling stages. The structures are heated by irradiation of the CNT-containing regions and cooled by convection of heat from the actuator surface.

A jellyfish-inspired CNT skeleton (Figure 1c) is combined with a PNIPAM hydrogel such that the VACNT forests are loaded with hydrogel and the bulk hydrogel is present both between each separate VACNT structure and as a ‘webbing’ between the actuator “tentacles”. This webbing is visible as a translucent material showing increased opacity at $>T_c$ (Figure 7). When observed from the top using laser powers $\approx 20 \text{ W cm}^{-2}$, the structures reversibly contract upon illumination (Figure 7a). Though typically pinned in place by the small observation cell, displacement of the structure is sometimes observed (Figure 7b). This displacement is unpredictable and it likely depends on a combination of multiple factors, including uncontrolled factors such as the position of the structure relative to the cell walls and pinning. Further optimization of the asymmetries in the forward and reverse strokes is likely needed to achieve reliable reproducible locomotion.

Side-on imaging of a larger observation cell reveals actuation behavior (Figure 7c), including different components of the jellyfish-like structure responding at different rates (Figure S10, Supporting Information). Curvature in the actuator results from

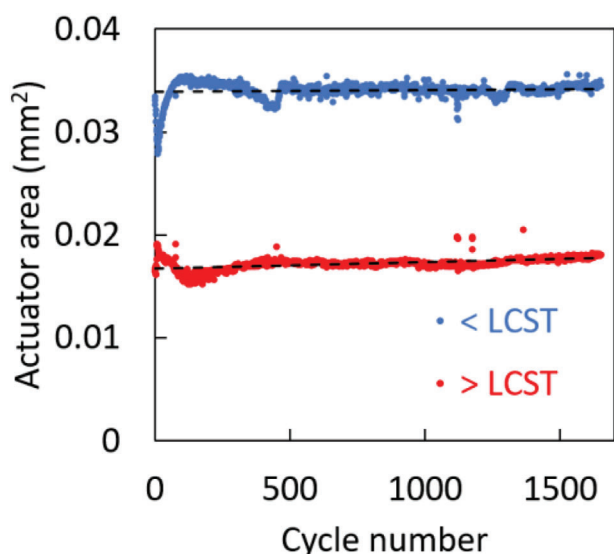


Figure 6. CNT/PNIPAM hydrogel microactuator when below (blue) and above (red) its lower critical solution temperature (LCST), as the actuator is cycled 1650 times through its swollen and contracted actuation states respectively. Negligible degradation is observed throughout cycling, suggesting that CNT/PNIPAM hydrogel actuators maintain $>80\%$ operation over more than 8,000 cycles.

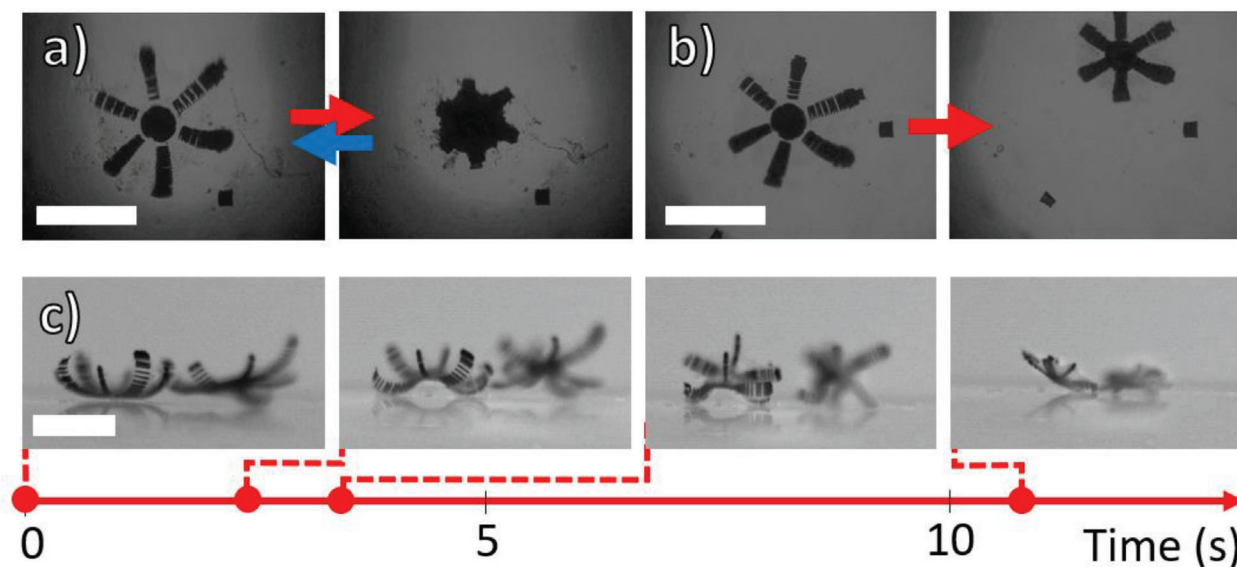


Figure 7. a,b) Transmission optical microscopy images of jellyfish-inspired CNT/hydrogel microactuator (top-view) showing a) typical actuation cycle and b) locomotion of a jellyfish-inspired actuator under contraction. c) Side-on images of IR LED-driven deswelling of jellyfish-inspired CNT/hydrogel swimmers, with timeline. Scale bars 1 mm.

the large hydrogel density at the base of the structure, which is a feature of this fabrication method. Larger observation cells require optical heating by large-area illumination with IR LEDs (as it is difficult to track a laser spot on the moving structure). Current high-power LEDs provide powers $<10 \text{ W cm}^{-2}$, resulting in slower actuation and no locomotion. While such CNT/PNIPAM hydrogel jellyfish-like actuators may be able to locomote by repeated actuation, the high-speed actuation that is desired requires unrealistic illumination for practical microswimmer applications. Optimal strategies from the kinetic model above particularly encourage shrinking the actuator size. Reducing the size of the jellyfish-like actuator is possible using our current approach of CNT skeletons, but hydrogel deposition requires further optimization for the reliable fabrication of complex morphologies on smaller scales.

3. Conclusion

Light-responsive microactuators composed of carbon nanotube and PNIPAM hydrogel composites are demonstrated to have response times of tens of milliseconds. The carbon nanotubes introduce high emissivity/absorptivity making light activation possible and the carbon nanotube skeletons allow for complex actuator shapes. The contraction kinetics of the composite actuators are strongly dependent on the network diffusion of the hydrogel polymer. A theoretical model for the actuator deswelling is developed, which shows that the composite response is significantly slowed by phase separation in the hydrogel. This theoretical model suggests strategies for improving actuation speed, including reducing the effects of phase separation and shrinking the initial size of the microactuators. Applications of CNT/hydrogel actuators as microswimmers are discussed, with promising early results showcasing their excellent cyclability, the ability to fabricate intricate structures, and a variety of complex behaviors.

4. Experimental Section

Patterned Growth of Vertically Aligned Carbon Nanotube Forests by Chemical Vapor Deposition: CNT microstructures were grown on silicon and fused silica wafers with a catalyst layer of 9 nm of Al_2O_3 and 1 nm Fe. The catalyst pattern was defined by photolithography using AZ5214E photoresist, and the catalyst materials were deposited using e-beam evaporation. The CNT forest was grown for 1–2 min in a horizontal tube furnace at atmospheric pressure using gas flows 100/400/100 $\text{C}_2\text{H}_4/\text{H}_2/\text{He}$.

Redox Polymerization and Crosslinking of N-Isopropylacrylamide: N-isopropylacrylamide (NIPAM) (255 mg) and N,N'-methylenebis(acrylamide) (BIS) (2.25 mg) were added to 1.5 mL of water. Nitrogen gas was bubbled through this monomer solution for at least 15 min to remove oxygen. Potassium persulfate (KPS) solution (85 μL of 60 mg mL^{-1} solution) and tetraethylenediamine (TEMED) (2.3 μL) were used as the initiator and accelerator respectively. A fresh KPS solution was made on the day to avoid degradation. UV-ozone treatment was used to hydrophilize the surface of the CNT sample to improve the wetting of the pre-polymer solution onto the CNT structures. After adding the KPS and TEMED, the prepolymer solution was swirled to make a homogeneous solution and deposited onto the treated CNT sample within 10 min. The solution was deposited either by drop casting and the samples were kept under nitrogen for at least 2 h for the polymerization reaction to complete.

Removing Composite Material from Substrate to Obtain Free Actuators: When the actuators were to be removed from the substrate, the prepolymer solution was deposited onto the sample in excess, such that the CNT structures were surrounded by bulk PNIPAM. Once polymerization was completed, the sample was left in water overnight to fully hydrate. The hydrogel expanded upon hydration such that the sample peeled itself away from the substrate to relieve the stress of the difference in size between the hydrogel and the substrate.

Light Actuation: The actuator was held in a chamber of water, which was placed on an optical microscope stage suitable for transmission imaging. A 532 nm laser was directed into the sample from below the stage, using a dichroic to reflect the laser upwards while still allowing the illumination white light to pass through for transmission imaging. A long-pass filter was placed before the microscope camera to block the laser beam, improving imaging and preventing damage to the camera. The incident optical power of the laser was varied from $\approx 10\text{--}55 \text{ W cm}^{-2}$.

Supporting Information

Supporting Information is available from the Wiley Online Library or from the author.

Acknowledgements

The authors thank experimental help and advice from Ermanno Miele and Megan Groom. The authors acknowledge support from the European Research Council (ERC) under Horizon 2020 research and innovation programme PICOFORCE (grant agreement no. 883703), MIGHTY (866005), and POSEIDON (grant agreement no. 861950). The authors acknowledge funding from UK EPSRC (EP/V050923/1, EP/N016920/1, Cambridge NanoDTC EP/L015978/1, EP/L027151/1, EP/S022953/1, EP/P029426/1, and EP/R020965/1).

Conflict of Interest

The authors declare no conflict of interest.

Data Availability Statement

The data that support the findings of this study are openly available in Apollo at 10.17863/CAM., reference number 100241.

Keywords

carbon nanotubes (CNTs), hydrogel, light actuation, microactuator, soft robotics, vertically aligned CNTs

Received: August 28, 2023

Revised: October 5, 2023

Published online:

- [1] A. Gregg, M. F. L. De Volder, J. J. Baumberg, *Adv. Opt. Mater.* **2022**, 10, 2200180.
- [2] E. Sato Matsuo, T. Tanaka, *J. Chem. Phys.* **1998**, 89, 1695.
- [3] M. Podewitz, Y. Wang, P. K. Quoika, J. R. Loeffler, M. Schauperl, K. R. Liedl, *J. Phys. Chem. B* **2019**, 123, 8838.
- [4] S. A. Deshmukh, S. K. R. S. Sankaranarayanan, K. Suthar, D. C. Mancini, *J. Phys. Chem. B* **2012**, 116, 2651.
- [5] L. Ionov, *Mater. Today* **2014**, 17, 494.
- [6] S.-J. Jeon, A. W. Hauser, R. C. Hayward, *Acc. Chem. Res.* **2017**, 50, 161.
- [7] M. De Volder, S. H. Tawfick, D. Copic, A. J. Hart, *Soft Matter* **2011**, 7, 9844.
- [8] B. Peng, M. Locascio, P. Zapol, S. Li, S. L. Mielke, G. C. Schatz, H. D. Espinosa, *Nat. Nanotechnol.* **2008**, 3, 626.
- [9] S. Ogata, Y. Shibutani, *Phys. Rev. B* **2003**, 68, 165409.
- [10] Y. Bai, H. Yue, J. Wang, B. Shen, S. Sun, S. Wang, H. Wang, X. Li, Z. Xu, R. Zhang, F. Wei, *Science* **1979**, 369, 1104.
- [11] M. R. Falvo, G. J. Clary, R. M. Taylor, V. Chi, F. P. Brooks, S. Washburn, R. Superfine, *Nature* **1997**, 389, 582.
- [12] J. Suhr, P. Victor, L. Ci, S. Sreekala, X. Zhang, O. Nalamasu, P. M. Ajayan, *Nat. Nanotechnol.* **2007**, 2, 417.
- [13] M. De Volder, S. H. Tawfick, S. J. Park, D. Copic, Z. Zhao, W. Lu, A. J. Hart, *Adv. Mater.* **2010**, 22, 4384.
- [14] K. Mizuno, J. Ishii, H. Kishida, Y. Hayamizu, S. Yasuda, D. N. Futaba, M. Yumura, K. Hata, *Proc Natl Acad Sci U S A* **2009**, 106, 6044.
- [15] Z.-u.-P.o Yang, L. Ci, J. A. Bur, S.-Y.u Lin, P. M. Ajayan, *Nano Lett.* **2008**, 8, 446.
- [16] K. Takahashi, T. Takigawa, T. Masuda, *J. Chem. Phys.* **2004**, 120, 2972.
- [17] T. Takigawa, T. Yamawaki, K. Takahashi, T. Masuda, *Polym J* **1999**, 31, 595.
- [18] T. Okajima, I. Harada, K. Nishio, S. Hirotsu, *J. Chem. Phys.* **2002**, 116, 9068.
- [19] T. Fujiyabu, F. Toni, X. Li, U.-I. Chung, T. Sakai, *Chem. Commun.* **2018**, 54, 6784.
- [20] K. Dušek, M. V. Dušková-Smrčková, *Gels* **2020**, 6, 22.
- [21] S. Cai, Z. Suo, *J. Mech. Phys. Solids* **2011**, 59, 2259.
- [22] R. Brighenti, M. P. Cosma, *J. Mech. Phys. Solids* **2022**, 169, 105045.
- [23] C. Xuan, L. Jin, *J. Mech. Phys. Solids* **2019**, 124, 599.
- [24] T. Tanaka, L. O. Hocker, G. B. Benedek, *J. Chem. Phys.* **1973**, 59, 5151.
- [25] T. Tanaka, D. J. Fillmore, *J. Chem. Phys.* **1979**, 70, 1214.
- [26] Y. Li, T. Tanaka, *J. Chem. Phys.* **1990**, 92, 1365.
- [27] M. Shibayama, T. Tanaka, *Adv. Polym. Sci.* **1993**, 109, 1.
- [28] M. Lehmann, P. Krause, V. Miruchna, R. Von Klitzing, *Colloid Polym. Sci.* **2019**, 297, 633.
- [29] M. A. Haq, Y. Su, D. Wang, *Mater. Sci. and Engineering C* **2017**, 70, 842.
- [30] S. Hirotsu, *Phase Transitions* **1994**, 47, 183.
- [31] Y.u Zhou, L. Jin, *Macromolecules* **2022**, 56, 426.
- [32] Y. Dogu, O. Okay, *J. Appl. Polym. Sci.* **2006**, 99, 37.
- [33] Q. Liu, P. Zhang, A. Qing, Y. Lan, M. Lu, *Polymer (Guildf)* **2006**, 47, 2330.
- [34] X. S. Wu, A. S. Hoffman, P. Yager, *J Polym Sci A Polym Chem* **1992**, 30, 2121.
- [35] T. Fujigaya, T. Morimoto, Y. Niidome, N. Nakashima, *Adv. Mater.* **2008**, 20, 3610.
- [36] A.-I. Bunea, D. Martella, S. Nocentini, C. Parmeggiani, R. Taboryski, D. S. Wiersma, *Adv. Intell. Syst.* **2021**, 3, 2000256.
- [37] E. M. Purcell, *Am. J. Phys.* **1977**, 45, 3.
- [38] E. Lauga, *Soft Matter* **2011**, 7, 3060.
- [39] A. Mourran, O. Jung, R. Vinokur, M. Möller, *Eur. Phys. J. E* **2021**, 44, 1.